Journal of Thermal Science Vol.26, No.2 (2017) 107−112

DOI: 10.1007/s11630-017-0917-8 **Article ID: 1003-2169(2017)02-0107-06**

Measurement and Numerical Simulation of a Small Centrifugal Compressor Characteristics at Small or Negative Flow Rate

Kaname Tsukamoto[1], Mizuki Okada[1], Yuzo Inokuchi[1], Nobuhiko Yamasaki[1] and Akihiro Yamagata[2]

1. Kyushu University, Motooka 744, 819-0395, Fukuoka, Japan,
2. IHI Corporation, Shin-Nakahara 1, 235-8501, Yokohama, Japan,

For centrifugal compressors used in automotive turbochargers, the extension of the surge margin is demanded because of lower engine speed. In order to estimate the surge line exactly, it is required to acquire the compressor characteristics at small or negative flow rate. In this paper, measurement and numerical simulation of the characteristics at small or negative flow rate are carried out. In the measurement, an experimental facility with a valve immediately downstream of the compressor is used to suppress the surge. In the numerical work, a new boundary condition that specifies mass flow rate at the outlet boundary is used to simulate the characteristics around the zero flow rate region. Furthermore, flow field analyses at small or negative flow rate are performed with the numerical results. The separated and re-circulated flow fields are investigated by visualization to identify the origin of losses.

Keywords: centrifugal compressor, turbocharger, measurement, CFD, RANS, surge, small flow, negative flow

Introduction

In recent years, automobile manufacturers attempt to improve the fuel efficiency by decreasing engine speed. Due to lower engine speed, for centrifugal compressors of automotive turbochargers, it is demanded to estimate the surge line exactly to extend the surge margin at smaller flow rate. The compressor characteristics at small or negative flow rate are required for the better understanding and modeling of the surge.

As Greitzer [1] explains, the surge can be modeled as a Helmholtz resonator, which implies that if the volume of the system is zero, there should be no resonance, i.e., no surge. According to this idea, Fink et al. [2] used a CCV, closed coupled valve, just downstream of the compressor to reduce the volume of the piping system. However, in the real system, we cannot make the volume of the piping system to exact zero as the theory does, and we cannot always avoid the surge, especially near the zero flow rate. This may be the reason why we can find few published data for the small flow rate cases that lies between the usual surge line and the zero flow rate line on the performance curve. The unstable nature of the surge is also observed in the numerical simulation, and this physical instability tends to diverge the steady state simulation near the zero flow rate. Marelli [3] et al. uses a throttle valve located upstream of the compressor, instead of a CCV located downstream as Fink et al. [2] did, and they replaced the upstream throttle valve to a blind flange in order to measure the zero flow rate characteristics. Galindo et al. [4] developed a 1DCAE code that predicts unsteady characteristics of a compressor, which uses the real performance map extended to the negative flow rate (extended performance map), in order to predict

Received: October 2016 Nobuhiko Yamasaki: Professor

the deep surge. Galindo et al. [4] uses the compressed air regulated by an orifice that is fed into the compressor from the usual 'outlet', so as to realize the negative flow rate condition. As they noted, this test is very destructive and to the best of our knowledge, there is no report other than Galindo et al. [4] for the negative flow rate measurement.

The objectives of our research are to carry out the measurement and numerical simulation when the compressor operates in the unstable conditions and to improve the precision of experimental measurements and numerical simulations by comparing each result, aiming to construct the method of predicting the surge in the future. In this paper, we report the measured and simulated results in the unstable conditions, where there seems no precedent for the simulation at negative flow rate.

Experimental facility

In the experimental work, a test bench to measure the compressor characteristics was set up with an automotive turbocharger for 1.4L gasoline engines. The compressor is a centrifugal one which has 6 full blades, 6 splitter blades, and a vaneless diffuser. The test bench is essentially the same with the facility introduced by Jung et al. [5], but a special modification is made this time to measure the small and negative flow rate range. Figure 1 shows the arrangement to measure the positive flow rate characteristics. The compressed air from the air tank drives the turbine and rotational speed is regulated with the control valve on the turbine side (Valve 1). The control valve on the compressor side (Valve 2) regulates flow rate through the compressor. In addition, the butterfly valve (Valve 3) is placed immediately downstream of the compressor to decrease the volume downstream of the compressor. In our previous facility, all we have done to decrease the volume downstream of the compressor is setting the position of Valve 2 in close proximity of the compressor. However, the characteristics at small flow rate could not be measured with such facility because Valve 2 is a globe valve, which essentially has the large internal volume. Therefore, the butterfly valve (Valve 3), which has the smaller internal volume is installed between the compressor and the globe valve (Valve 2) this time. Whereas the butterfly valve (Valve 3) is open in the test at large flow rate, it is almost closed to suppress the surge in the small flow rate test. The length of the duct between the compressor outlet and the butterfly valve is 4.2D, where D is the diameter of the outlet duct. Flow rate is measured with the thermal flowmeter on the inlet duct of the compressor. Pressure and temperature are measured at the measurement points on the inlet and outlet ducts. The piezo resistive pressure sensors and the K-type thermocouples are used. Rotational speed is measured with the magnetic sensor which senses the magnetic field variation caused by the magnetized nut attached on the compressor shaft. The experimentally obtained performance curves in this paper show averaged values whose sampling time and frequency are 3 seconds and 71.43 kHz, respectively.

Figure 2 shows the arrangement of the negative flow rate test. The compressed air in the air tank flows to the compressor outlet duct while it also drives the turbine. In the negative flow rate test, the control valve on the compressor side (Valve 2) is closed. Flow rate through the compressor is regulated with the butterfly valve (Valve 3) and the pressure regulator on the duct that connects the air tank and the compressor outlet duct (Valve 4).

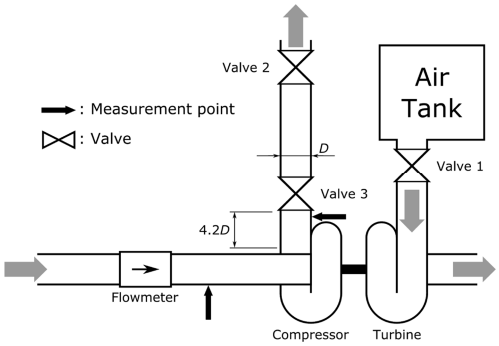

Fig. 1 Test bench configuration for the positive flow rate test.

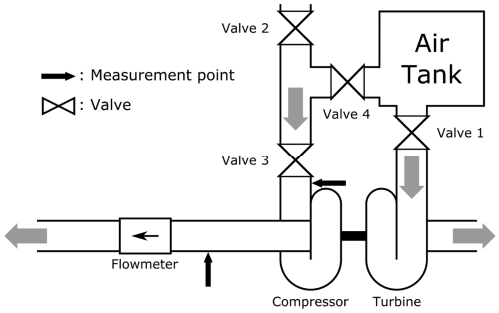

Fig. 2 Test bench configuration for the negative flow rate test.

Numerical method

Figure 3 shows the compressor model used in the numerical analysis. This model is based on the turbocharger compressor used in the experimental work. At the maximum rotational speed in this study, Reynolds number based on the span length of the full blade is about 1.3×10^5 and Mach number is about 0.5 in the rotating frame of reference. All results shown in this paper are steady state results.

The fluid flow solver is the UPACS-turbo developed by JAXA, Japan Aerospace Exploration Agency, which uses the cell-centered finite volume method. The governing equation is the compressible RANS and the Spa-

lart-Allmaras turbulence model is used in this study. The Roe scheme is used for the convective terms, while viscous terms are discretized by the second order centered scheme. The first order Euler implicit method is used for time integration, in which the algebraic equations with a large sparse matrix is solved by the matrix free Gauss Seidel method. Spatially varying time stepping method is used and CFL number is 40.0.

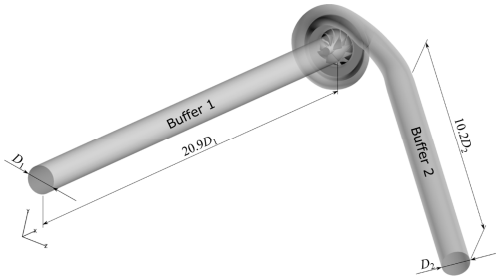

Fig. 3 CFD domain.

The grid mesh system is structured multi-block meshes. The total number of cells is about 15.80M, in which 0.97M cells for one pitch of the impeller, 1.64M cells for the diffuser, and 4.99M cells for the volute. The buffer ducts are placed in order to place the boundaries at a position where no reversal flow exists and in order to dump undesired acoustic reflections from the boundaries. The length of the buffer duct adjacent to the impeller domain (Buffer 1) is $20.9D_1$, where D_1 is its diameter. The length of the buffer duct adjacent to the volute domain (Buffer 2) is 10.2 D_2, where D_2 is the diameter of the volute outlet. The number of cells for the buffer ducts is 3.37M. The minimum grid spacing normal to the impeller blade is about 1.9×10^{-5}, where the length is non-dimensionalized by the span length of the full blade at the leading edge.

The boundary conditions are given as follows. Total pressure and temperature at the inlet boundary are specified as the atmospheric values. The inlet boundary is the one on the Buffer 1 in the positive flow rate simulation, whereas it is the one on the Buffer 2 in the negative flow rate simulation. The non-slip and adiabatic conditions are applied to the solid walls. At the outlet boundary, either static pressure or mass flow rate is specified. If the operating point is far from the zero flow rate line, static pressure is specified. On the other hand, if it is near to the zero flow rate line, mass flow rate is specified. In this method, five primitive variables at the outlet boundary are calculated based on the characteristic theory under the constraint of the specified mass flow rate, and are relaxed to dump the acoustic wave reflections [6]. Length, velocity, and density are scaled by L, c_∞, and ρ_∞, respectively, where L is the full blade span length at the leading edge, c_∞ and ρ_∞, are speed of sound and density at the reference condition (inlet condition in this study), and γ is specific heat ratio. Therefore, non-dimensional pressure of the atmospheric condition has the value of $1/\gamma$~0.714, and non-dimensional mass flow rate is scaled by $\rho_\infty c_\infty L^2$.

Results and discussion

The measured and calculated performance curves are shown in Fig. 4. The triangle and circle symbols denote the measured and calculated operating points, respectively. The abscissa is volumetric flow rate which is non-dimensionalized by the maximum value in the experimental work ($Q_{\mathrm{exp,max}}$). The ordinate is pressure ratio where total pressure measured upstream and downstream of the compressor are used. Mu_2 in the figure denotes rotational Mach number defined as $Mu_2=U_2/a_\infty$, where U_2 is rotational speed of the impeller and a_∞ is speed of sound in the standard condition. Flow rate, pressure ratio, and rotational Mach number are the corrected values, i.e., pressure and temperature are reduced to the values at the standard condition.

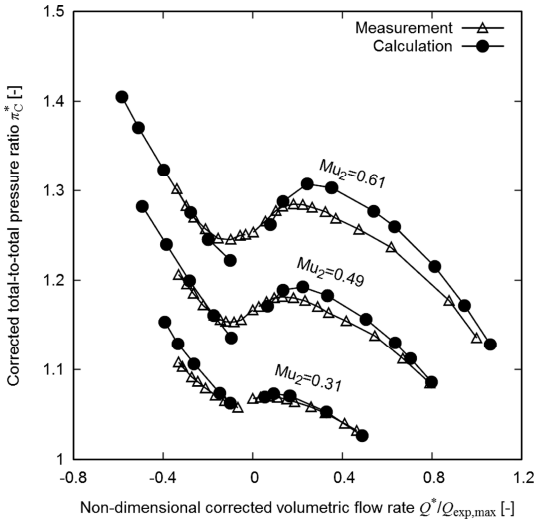

Fig. 4 Comparison of the performance curves between the measurement (triangle) and the calculation (circle).

The operating points in the unstable flow region can be measured by decreasing volume downstream of the compressor. According to Greitzer [1], the instability of a compressor depends on a non-dimensional parameter (B), which is related to Helmholtz frequency. The B parameter is defined as

$$B=\frac{U}{2a}\sqrt{\frac{V_p}{A_C L_C}} \tag{1}$$

where U, a, V_p, A_C, and L_C denote mean rotational velocity, speed of sound, exit plenum volume, duct cross section area, and duct length, respectively. The smaller B tends to stabilize the compressor system in the small or

negative flow rate regions. The placement of the butterfly valve immediately downstream of the compressor decreases the V_p or B, and that allows the characteristics in the unstable flow rate regions to be measured.

The characteristics at small or negative flow rate can be simulated by using the mass-flow-specified boundary condition. In the positive flow rate region, when compared between the measurement and calculation, the calculation tends to overestimate both pressure ratio and flow rate of the peak characteristics particularly at high rotational speed. On the other hand, in the negative flow rate region, the calculated characteristics far from the zero flow rate region show good agreement with the measured ones, whereas the calculation tends to underestimate pressure ratio near the zero flow rate.

Figure 6 shows the visualization results for the simulation cases (a), (b), and (c) on the performance curve of Fig. 5, and labels (a), (b), and (c) on Fig. 6 corresponds to the labels (a), (b), and (c) on Fig. 5, respectively. The figure with sub-label (1) shows the non-dimensional static pressure contour on the impeller. The figures with sub-labels (2) and (3) show the streamlines from different viewpoints. The streamlines are drawn based on the relative velocity vector, and the thickness of the line indicates the velocity magnitude. The streamlines from the tip of the leading edge of the full-blade are colored with pale blue, while those from the splitter blade tip are colored with purple. The seeds of 10 points are injected in the radial and circumferential directions between the full blades, and the streamlines from the seeds in the radial direction are colored with dark orange, while those from the seeds in the circumferential direction are colored with dark yellow. The streamlines are drawn by integrating the velocity vector only in the downstream direction for the cases (a) and (b), while in the case (c) the streamlines are integrated both in the upstream and downstream directions, to show their features clearly. The figure with sub-label (4) shows the contour of entropy function on the four cross-sections. The three of four cross sections are almost perpendicular to the passage and are located near the inlet of the impeller, near the leading edge of the splitter blade, and near the trailing edge. The remaining cross section is almost parallel to the passage and located near the mid-span. The definition of entropy function is $s^*=\exp(\Delta s/R)$, which is equal to 1 when there is no entropy change. Entropy function increases exponentially as entropy increases, which can be used to quantify the generation of the loss in the flow field.

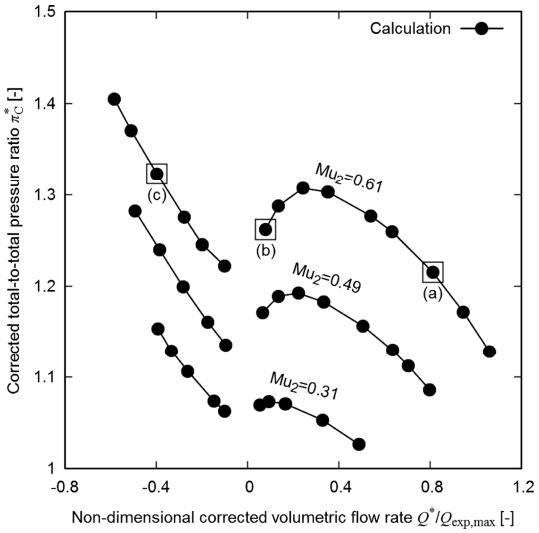

Fig. 5 Performance curves in the calculation. The three points in the square indicate the operating points used in the flow field analyses: (a), (b), and (c) indicates the stable flow, the small flow, and the negative flow, respectively.

In the stable flow region of case (a), static pressure increases from the leading edge to the trailing edge, as shown in Fig. 6 (a1). The low pressure region near the leading edge of the full blade near the tip on the suction side is caused by the flow acceleration on the suction side. The flow passes with almost no separation of the flow, as shown in Fig. 6 (a2) and (a3). The loss in this flow is very small almost in the whole region of the passage except near the casing wall, as shown in Fig. 6 (a4).

In the small flow rate region of case (b), which has the lower flow rate than the surge line flow rate, Fig. 6 (b1) shows that the static pressure increases from the hub to the casing, and there is large pressure gradient in the span direction, while in the stable region of case (a) the pressure gradient is observed in the chord direction. Fig. 6 (b2) and (b3) show that only the flow near the hub-side passes through the blades and the flow near the casing separates to produce the reverse flow. As a result, the recirculation flows from the casing flow to the hub flow are formed, which makes the loss near the inlet of the impeller higher than the case (a) shown in Fig. 6 (a4). The flow stalls due to the adverse pressure gradient near the trailing edge, which can be recognized by the curvature of the dark yellow streamlines, that makes the loss in the passage higher.

In the negative flow rate region of case (c), the pressure gradient is observed in the span direction as in the small flow rate region of case (b). However, when the contour range is adjusted to be the same as the cases (a) and (b), the pressure gradient in the case (c) cannot be recognized clearly, as shown in Fig. 6 (c1). In the negative flow rate region, the flow comes from the volute to the diffuser and hits the pressure side near the trailing edge, as shown in Fig. 6 (c2) and (c3), which makes the wall pressure near the trailing edge extremely higher than other cases of (a) and (b), as shown in Fig. 6 (c1). At the same time the flow near the trailing edge produces large scale separation on the suction side, which forms large vortex structure inside the passage, as is observed in Fig. 6 (c3). The flow passes from the trailing edge to the

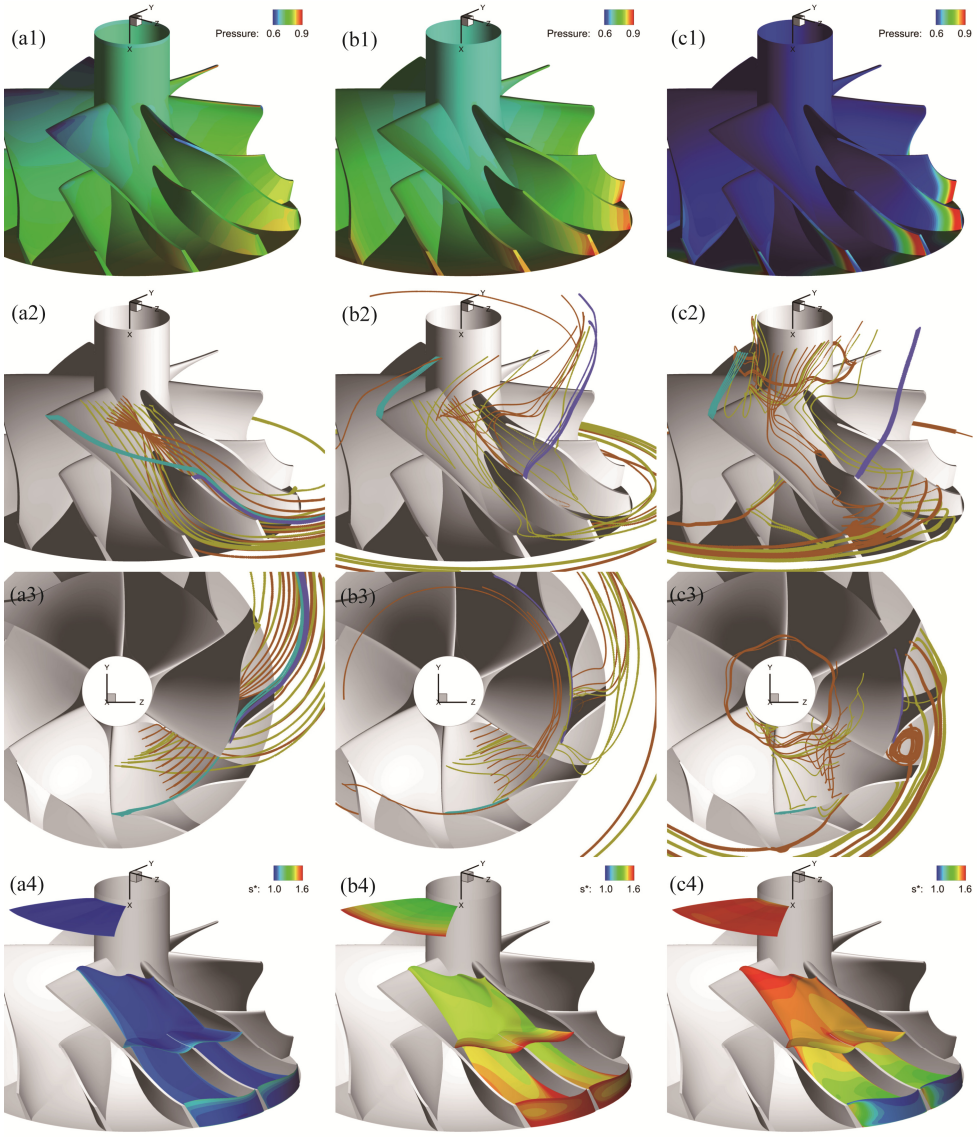

Fig. 6 Flow visualization for the simulation cases of (a), (b), and (c) in Fig. 5. The figures with sub-number (1) shows the non-dimensional static pressure contour, (2) and (3) the streamlines, and (4) entropy function.

leading edge, and the swirling flow produced by the impeller flows from the leading edge to the inlet of the impeller. The loss is the highest near the inlet in this case.

Conclusion

In this study, both the experimental and numerical work were carried out to estimate the small or negative flow rate characteristics of the turbocharger compressor for automotive engines. In the experimental work, the special facility equipped with the butterfly valve immediately downstream of the compressor allows the characteristics to be measured. In the numerical work, the CFD simulation was carried out in the same conditions as the experiment. The new boundary condition which specifies mass flow rate at the outlet boundary allows the simulation in the unstable flow region. In addition, the flow fields around the impeller at small or negative flow rate were visualized. At small flow rate, the flow separation is occurred near the casing and the flow stalls due to the adverse pressure gradient near the trailing edge. As a result, the loss near the inlet of the impeller and in the passage is higher than the stable flow region. At negative flow rate, the large vortex structure and the swirling flow are formed inside the passage, and the loss is the highest near the inlet of the impeller.

Acknowledgement

We are deeply grateful to Dr. Kazuomi Yamamoto and

Dr. Junichi Kazawa, Japan Aerospace Exploration Agency, for providing the UPACS-turbo code with mass-flow specification capability.

The computation was mainly carried out using the computer facilities at Research Institute for Information Technology, Kyushu University.

References

[1] Greitzer, E. M.: Surge and rotating stall in axial flow compressors Part: I: Theoretical compression system model, Journal of Engineering for Power, vol.98, No.2, pp.190–198, (1976).

[2] Fink, D. A., Cumpsty, N. A., and Greitzer, E. M.: Surge dynamics in free-spool centrifugal compressor system, Journal of Turbomachinery, vol.114, No.2, pp.321–332, (1992).

[3] Marelli, S., Carraro, C., Marmorato, G., Zamboni, G., and Capobianco, M.: Experimental analysis on the performance of a turbocharger compressor in the unstable operating region and close to the surge limit, Experimental Thermal and Fluid Science, Vol.53, pp.154–160, (2014).

[4] Galindo, J., Serrano, J. R., Climent, H., and Tiseira, A.: Experiments and modelling of surge in small centrifugal compressor for automotive engines, Experimental Thermal and Fluid Science, vol.32, pp.818–826, (2008).

[5] Jung, M., Nagayama, Y., Umeno, H., Inokuchi, Y., Yamasaki, N., Yamagata, A.: Experimental research on the transient surge of automotive turbochargers, Proc. Asian Joint Conference on Propulsion and Power, Jeju, Korea, AJCPP2014-097 (8 pages) (2014).

[6] Yamamoto, K., Horiguchi, Y., and Aotsuka, M.: A mass flow boundary condition for compressible flow computations, Proc. 45th Fluid Dynamics Conference/ Aerospace Numerical Simulation Symposium 2013, Tokyo, Japan, JSASS-2013-2039-A (7 pages) (2013) (in Japanese).